

*Chapter 3*

**ALPHA-PARTICLE RADIOBIOLOGICAL EXPERIMENTS  
INVOLVING SOLID STATE NUCLEAR TRACK  
DETECTORS AS SUBSTRATES**

***K. N. Yu and D. Nikezic***

Department of Physics and Materials Science, City University of Hong Kong,  
Tat Chee Avenue, Kowloon, Hong Kong.

**ABSTRACT**

Alpha-particle radiobiological experiments involve irradiating cells with alpha particles and require accurate positions where the alpha particles hit the cells. For such purposes, solid state nuclear track detectors (SSNTDs) such as cellulose nitrate films or polyallyldiglycol carbonate (PADC) films can be used as support substrates. PADC films have various advantages and these will be the focus of the present chapter. However, sufficiently thin (<20  $\mu\text{m}$ ) PADC films required in radiobiological experiments are not commercially available and their fabrication is a challenge. Although procedures based on UV-curing have been developed to fabricate thin PADC films, these require specialized expertise and dedicated equipment. As such, the present chapter is devoted mainly to the discussion on the thin PADC films fabricated by etching commercially available thick PADC films. Section 2 gives details on the preparation of thin PADC films (<20  $\mu\text{m}$ ) from commercially available CR-39 SSNTDs with a thickness of 100  $\mu\text{m}$ . The optimal etching conditions are to use 1 N NaOH/Ethanol at 40 °C as the etchant, for which the desired final thickness can be achieved for ~ 8 h. Such etching conditions can yield the desired thin PADC films within a reasonably short time, while providing relatively transparent and less rough PADC films for radiobiological experiments which require observations under the optical microscope. Section 3 describes two applications of the fabricated thin PADC films, namely, for alpha-particle irradiation of cell cultures and for alpha-particle irradiation of zebrafish embryos. Finally, section 4 examines the biocompatibility of the PADC film substrates, which is a key factor to the success of radiobiological experiments. In particular, the biocompatibility of chemically etched PADC films, and the biocompatibility enhancement of chemically etched PADC films through superficial pore formation will be discussed.

## 1. INTRODUCTION

Alpha-particle radiobiological experiments are of interest because alpha particles are an ionizing radiation with high linear energy transfer, and alpha particles are emitted from radon and its progeny, which are ubiquitous in our natural environment and constitute the largest natural radiation dose to human and can induce lung cancers. These alpha-particle radiobiological experiments involve irradiating cells with alpha particles and require accurate positions where the alpha particles hit the cells. The cells can refer to those in cell lines for *in vitro* experiments or those in *in vivo* models such as the zebrafish embryos.

To quantify the alpha-particle dose received by cells in both *in vitro* or *in vivo* experiments, alpha-particle hit positions are needed. For such purposes, solid state nuclear track detectors (SSNTDs) such as cellulose nitrate films and polyallyldiglycol carbonate (PADC) films can be used as support substrates. A review on SSNTDs has been given by Nikezic and Yu (2004). In most cases, it is only feasible to quantify the alpha-particle energies incident on the cells if the alpha particles pass through the substrate to strike the cells, because there is always a fluid layer with variable thickness above the cells. As such, the SSNTD employed as the support substrate should be thin enough to allow passage of alpha particles with nominal energies.

Durante et al. (1994) proposed a method based on application of the LR 115 film, the active layer of which was cellulose nitrate. They seeded two different rodent embryo fibroblast cell lines, namely C3H 10T1/2 and V79, on mylar films and LR 115 SSNTDs. Irradiation was performed with 3.2 MeV alpha particles from below the substrate. Experiments also included observations of the cells with a microscope connected to a video camera and an image analyzer. It was possible to measure the number of alpha-particle traversals through the cell nucleus or cytoplasm. The coordinates of each cell on the microscope bench were saved. After incubation for about one week, the cells were fixed and stained, and the colonies observed under the microscope. The fate of each irradiated cell was then correlated with the number of traversals. The studied endpoint was cell killing. It was found that only a few alpha-particle traversals were sufficient to kill the V79 cells. Here, it should be noted that a mylar film was applied between the cells and the detector because the LR 115 SSNTD itself was biologically incompatible.

Dorschel et al. (2003) then investigated the performance of the LR 115 SSNTD for radiobiological experiments. The basic experimental setup was similar to that of Durante et al. (1994). They noticed that the red dye from the LR 115 SSNTD could diffuse into the medium that was conditioning the cells. Because of this, they proposed to use the colorless LR 115 SSNTDs, which could be obtained from the manufacturer of the red LR 115 SSNTDs (DOSIRAD) upon special request. The characteristics of the colorless LR 115 SSNTD were also studied, including the bulk etch rate, energy window, track diameter, track length, critical angle, etc. The influence of ultraviolet (UV) irradiation, which was applied to sterilize the detector before the cells were seeded, was also examined. The authors found that the LR 115 SSNTD could be a feasible substrate for cell culture and for cell irradiation in radiobiological experiments. In the application of the red LR 115 SSNTD, a mylar foil between the detector and cell culture should be used. The colorless LR 115 SSNTD was also found to have similar detection characteristics as the red one, but for the colorless one, the surface quality was

worse and the relatively high background noise (in terms of tracks) complicated the identification and counting of real tracks.

Chan et al. (2006) further studied the feasibility of colorless LR 115 SSNTDs for alpha-particle radiobiological experiments. They found that the track revelation time on the bottom side (the side attached to the polyester base) was much longer than that on the top side (the side not attached to the polyester base) of the active layer so track formation on the top side was more desirable. In relation to this, culture of HeLa cells on the bottom side of the active layer was found feasible although the cultured cell number was relatively smaller. The feasibility of using this SSNTD for alpha-particle radiobiological experiments was demonstrated by culturing cells on the bottom side while performing alpha-particle irradiation and chemical etching on the top side, and by taking photographs of the cells and alpha-particle tracks together under the optical microscope.

To conclude, the relatively poor biocompatibility of the LR115 SSNTDs, together with the diffusion of red dye for the red detectors and the poor quality of tracks on the colorless detectors, have made their applications less straightforward. Another SSNTD which has been extensively explored as support substrates for radiobiological experiments is PADC (commercially available as the CR-39 detector). PADC films have many advantages. For example, they are transparent, more biocompatible and are not dissolved in the alcohol used for sterilizing the substrate. Therefore, the present chapter will be devoted to the discussion on application of PADC films as support substrates. However, as mentioned on the outset, the substrate should be thin enough to allow passage of alpha particles with nominal energies (e.g., those from  $^{241}\text{Am}$  source). According to the SRIM program (<http://www.srim.org/>), the range of 5 MeV alpha particles in PADC is 28.77  $\mu\text{m}$ . Unfortunately, the thinnest commercially available PADC films are  $\sim 100$   $\mu\text{m}$  thick and are thus not thin enough.

Gaillard et al. (2005) were the pioneers to fabricate ultra-thin PADC films as support substrates for cell cultures. They developed special procedures based on UV-curing to produce PADC films with a thickness of 10  $\mu\text{m}$ , which were grafted onto thin polyethylene terephthalate (PET) foils. The thin double polymeric layer was then used as the dish base. Human primary cells were successfully grown in these PADC-PET dishes. The positions of alpha-particle traversals could be obtained by etching the dish base for 2 h, and  $\alpha$ -particle-induced  $\gamma$ -H2AX foci were observed simultaneously with the etched tracks (Gaillard et al. 2005). These specialized dishes were used subsequently for studying the distance distribution of bystander effects in alpha-particle irradiated cell populations (Gaillard et al., 2008).

Nevertheless, these fabricated PADC films are not commercially available, and fabrication of these thin PADC films will require specialized expertise and dedicated equipment, which might not be easily available to all laboratories trying to perform alpha-particle radiobiological experiments. As a result, it is still desirable if methodologies can be explored and devised to fabricate sufficiently thin PADC films from thicker commercially available PADC films, e.g., those with a thickness of 100  $\mu\text{m}$ . The rest of the current chapter will be dedicated to discussions on an established method to fabricate thin PADC films (section 2) and on applications of these thin PADC films (section 3). The last section (section 4) will discuss the biocompatibility of the PADC films, which is a key factor to the success of radiobiological experiments.

## 2. FABRICATION OF THIN PADC FILMS FROM COMMERCIAL PADC FILMS

Chan et al. (2007a) prepared thin PADC films from commercially available CR-39 SSNTDs with a thickness of 100  $\mu\text{m}$  (purchased from Page Mouldings (Pershore) Limited, Worcestershire) by etching them in 1 N NaOH/Ethanol at 40°C to below 20  $\mu\text{m}$ .

For successful preparation of these thin PADC films, the bulk etch characteristics were studied in details (through the bulk etch characteristics of thicker CR-39 SSNTDs also from Page Mouldings). For etching PADC films in NaOH/Ethanol, a layer of precipitate consisting of sodium carbonate (which is one of the etched products) always accumulates on the surface of the PADC films (Tse et al. 2007). In order to ensure the most even and the fastest etching, the PADC films were regularly rinsed with distilled water every 2 h during etching in NaOH/Ethanol. The bulk etch rates of PADC films etched in NaOH/Ethanol were found to range from 22 to 75  $\mu\text{m}/\text{h}$  for different molarities at 55 °C as shown in Table 1. Therefore, the desired final thickness of 20  $\mu\text{m}$  could be achieved within as short as  $\sim 4$  h. However, such fast etching rates might result in excessive precipitation of etched products on the detector (Tse et al. 2007) leading to uneven etching. Finally, Chan et al. (2007a) chose the etchant as 1 N NaOH/Ethanol at 40 °C, for which the bulk etch rate of PADC films was  $\sim 10$   $\mu\text{m}/\text{h}$ . Under such etching conditions, the desired final thickness could be achieved for  $\sim 8$  h.

The roughness of the PADC films is of great concern for radiobiological experiments since a rough and opaque detector will hinder the study of radiobiological effects under the optical microscope. Therefore, the roughness of the prepared thin PADC films was studied by Chan et al. (2007a) using the atomic force microscope (AFM), and summarized in Table 2 here. PADC films etched in NaOH/Ethanol were rougher than those etched in 6.25 N NaOH/water solution, and the roughness increased with the molarities of NaOH/Ethanol. This supported the choice of Chan et al. (2007a) for the relatively mild etching conditions as 1 N NaOH/Ethanol at 40 °C, which could provide relatively transparent and less rough PADC films for radiobiological experiments which required observations under the optical microscope.

On the other hand, the track formation time should also be short since it would be desirable to be able to locate the hit positions of the cells within a very short time after irradiation. This is particularly difficult if the cells have to be kept alive at the same time so the etching temperature will need to be at 37 °C to match that required for cell culture. The track formation time is expected to be long for such a low etching temperature. Chan et al. (2007a) made use of UV irradiation to shorten track formation time on these thin PADC films. After exposure to UV light (UVA+B radiation) from a solar simulator for 2 to 3 h with doses from 260 to 390  $\text{mW}/\text{cm}^2$ , 5 MeV alpha-particle tracks could be seen to develop on these PADC films clearly under the optical microscope within 2 h in 14 N KOH at 37°C. KOH was used as the etchant because it was more reactive than NaOH and could reveal tracks within a shorter time frame.

After UV irradiation, the 20  $\mu\text{m}$  PADC films were glued by epoxy to the bottom of petri dishes with a diameter of 5 cm, with a hole of 1 cm diameter drilled at the bottom, to form the cell dishes as shown in Figure 1.

As an example for practical use, the custom-made petri dishes described above were used for culturing HeLa cervix cancer cells (Chan et al. 2007a). After cell cultivation, the PADC

cell dishes were irradiated from the bottom with 5 MeV alpha particles from an  $^{241}\text{Am}$  source (with the final alpha-particle energy incident on the PADC film controlled by the source to detector distance in normal air) under normal incidence through a collimator for a 1 h as depicted in Figure 2.

**Table 1. The bulk etch rates of PADC films in different etchants.  
(from Chan et al. 2007a.)**

Etchant	Bulk etch rate ( $\mu\text{m/h}$ )
0.5 N NaOH/ethanol at 55 °C	$22.4 \pm 0.7$
1.0 N NaOH/ethanol at 55 °C	$47.7 \pm 1.2$
1.5 N NaOH/ethanol at 55 °C	$61.3 \pm 3.7$
2.15 N NaOH/ethanol at 55 °C	$75.6 \pm 4.4$
2.52 N NaOH/ethanol at 55 °C	$75.3 \pm 2.6$
1.0 N NaOH/ethanol at 40 °C	$9.49 \pm 0.04$
1.5 N NaOH/ethanol at 40 °C	$11.7 \pm 0.1$

**Table 2. Root-mean-square (RMS) roughness of the PADC films etched with different etchants at 55 °C for 2 h. (from Chan et al. 2007a.)**

Etchant	RMS roughness from AFM
0.5 N NaOH/ethanol	0.00537
1.0 N NaOH/ethanol	0.00558
1.5 N NaOH/ethanol	0.00760
None	0.00261
6.25 N NaOH/water	0.00442

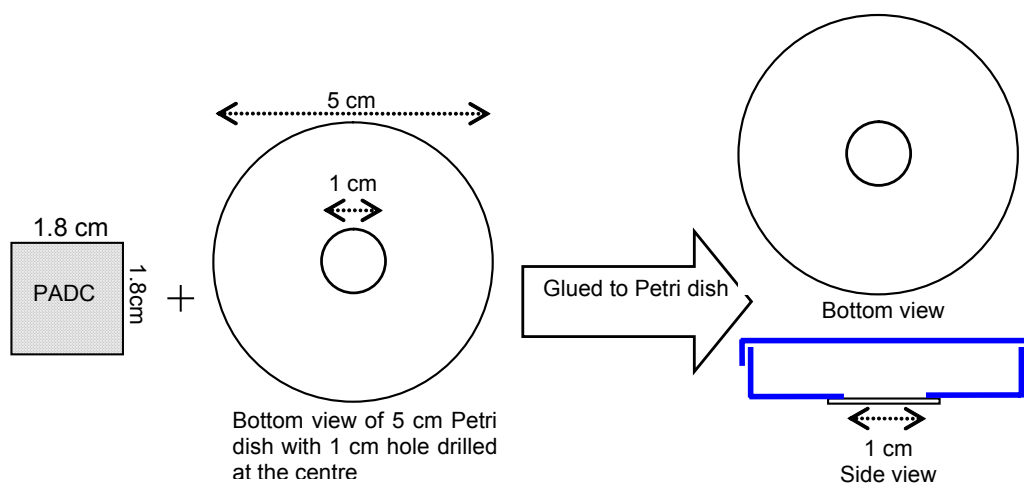


Figure 1. Preparation of thin PADC cell dish by gluing the thin PADC film onto the bottom of the Petri dish with 5 cm diameter and with a 1 cm hole drilled at the center of the bottom.

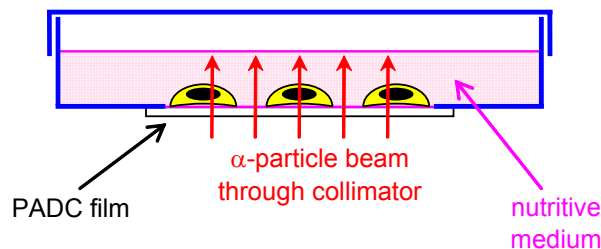


Figure 2. The irradiation of the cell monolayer through the custom made PADc cell dish. (Adopted from Chan et al. 2007a.)



Figure 3. The image of the HeLa cell monolayer on a thin PADc film with revealed alpha-particle tracks under the optical microscope with a magnification of 200 $\times$  (taken from the side of the cell monolayer). The 5 MeV alpha-particle tracks are seen on the right hand side as black dots. These tracks are developed on the underside of the PADc film (which is glued to the bottom of the cell dish) after chemical etching in (while floating on) a 14 N KOH solution at 37  $^{\circ}$ C for 4 h. (Adopted from Chan et al. 2007a.)

After alpha-particle irradiation, the PADc cell dish covered with the lid (with the cell culture inside) was kept floating on the 14 N KOH solution at 37  $^{\circ}$ C, leaving merely the bottom of the thin PADc film in contact with the etchant until the formation of visible tracks under optical microscope (Chan et al. 2007a). With the tracks revealed beneath the cell monolayer, the hit positions on the cell could be pinpointed under the optical microscope. The corresponding radiobiological effect on the cell could then be monitored.

The feasibility of using these thin PADc films was demonstrated by taking photographs of the cells and alpha-particle tracks together under the optical microscope, which could allow the hit positions on the cells by the alpha particles to be determined accurately. Figure 3 shows the image of a HeLa cell monolayer on a prepared piece of thin PADc film obtained by Chan et al. (2007a) under the optical microscope in the transmission mode with a magnification of 200 $\times$ . The image shows a group of alpha-particle tracks formed by etching the underside of the thin PADc film beneath the cell monolayer. This thin PADc film was exposed to UV light for 3 h before culturing the cells, and the cell dish was kept floating on the 14 N KOH solution for 4 h at 37  $^{\circ}$ C. The image shows both the positions of the alpha-particle tracks and the cells clearly, so location of hit positions on the cells by the alpha particles can be performed accurately. In fact, the tracks started to be observable in less than 2

h of etching under the optical microscope. A longer etching time (4 h) was used here to produce larger tracks that are more conspicuous on the shown image.

### **3. EXAMPLES OF ALPHA-PARTICLE RADIOBIOLOGICAL EXPERIMENTS INVOLVING THIN PADC FILMS AS SUPPORT SUBSTRATES**

#### **3.1. PADC Cell Dishes for Alpha-Particle Irradiation of Cell Cultures**

Chan et al. (2007b, 2008) employed custom-made petri dishes with ~20  $\mu\text{m}$  thick PADC films as cell-culture substrates to study the effect of alpha-particle irradiation on HeLa cervix cancer cells in terms of creation of DNA strand breaks. The thin PADC films were prepared from commercially available CR-39 SSNTDs as described by Chan et al. (2007a) and summarized in section 2 above. As previously explained, the PADC films recorded the positions where the alpha particles hit the cultured cells. Alpha particles with an energy of 5 MeV from an  $^{241}\text{Am}$  source were irradiated from the bottom of the PADC film. The hit frequency of cells by alpha particles was obtained from the positions of the etched alpha-particle tracks.

Chan et al. (2008) proposed a special method involving “base tracks” for aligning the images of cells and alpha-particle hits. After alignment, two sets of images were superimposed to obtain accurate positions of alpha-particle hits on the cells. The first set contained images of cells while the second set contained images of the tracks corresponding to the 5 MeV alpha particles used to irradiate the cells. Before culturing cells onto the custom-made cell dishes, the bottom of the PADC films were irradiated by 1 MeV alpha particles for 10 min. After irradiation, the bottom side of the cell dishes was etched by 14 N KOH solution at 37 °C to reveal the tracks. Such a low etching temperature was chosen to prevent the epoxy from being dissolved in the strong etchant at high temperatures. These tracks were used as markers for alignment only, and are referred to as “base tracks”. The tracks formed on the PADC films by 1 and 5 MeV alpha particles after chemical etching showed distinct characteristics and were thus conveniently distinguished from one another. For example, 1 MeV alpha-particle tracks had larger track openings and were shallower than 5 MeV alpha-particle tracks.

After introducing the markers, the PADC cell dishes were used for culturing HeLa cervix cancer cells. Images of these cells together with the markers were captured, and were referred to as the CM (cells and markers) images. The PADC cell dishes, with the cells inside, were then irradiated from the bottom with 5 MeV alpha particles under normal incidence through a collimator. During irradiation, some of the energy of the alpha particles will be absorbed while passing through the PADC film. The absorbed energy depended on the thickness of the PADC film, and the residual energy of the alpha particles after passing through the PADC film could be calculated using the SRIM program. In order to investigate the response of the cells to different alpha-particle energies, PADC films with various thicknesses were used in the experiments that would be subjected to irradiation of 5 MeV alpha particles (Chan et al. 2007b).

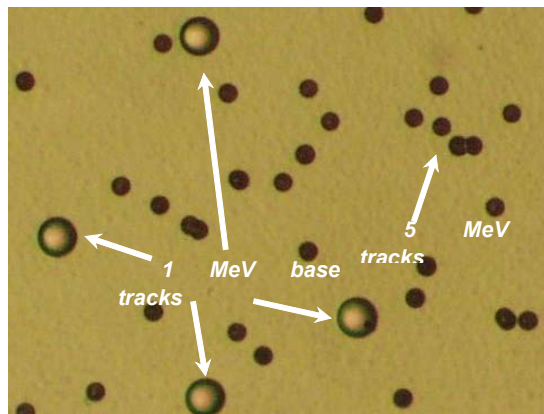


Figure 4. The images (with a magnification of 200 $\times$ ) of base tracks formed from 1 MeV alpha particles that have been etched for a cumulative period of 9 h 40 min, together with the images of tracks from 5 MeV alpha particles that have been etched for 6 h in 14 N KOH solution at 37  $^{\circ}$ C. (Adopted from Chan et al. 2007b.)

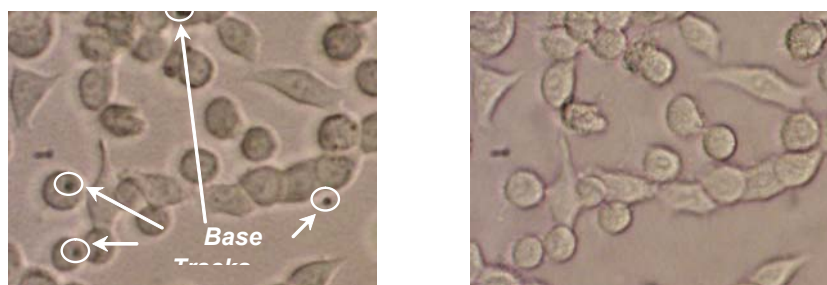


Figure 5. The images of base tracks from 1 MeV alpha particles with HeLa cells on the surface of the PADC film with a magnification of 200 $\times$ : (a) with focus on the tracks, and (b) with focus on the cells. (Adopted from Chan et al. 2007b.)

Chan et al. (2007b, 2008) used the TdT-mediated dUTP Nick-End Labeling (TUNEL) fluorescence method to detect the DNA strand breaks. Here, the enzyme TdT (terminal deoxynucleotidyl transferase) catalyzes the addition of fluorescein-labeled dUTPs (DeoxyUridine Triphosphate) to the free 3'-OH DNA ends in a template-independent manner. The fluorescein labels incorporated in nucleotide polymers are then detected and quantified by flow cytometry. Flow cytometry characterizes single cells as they pass through a laser beam at high speed. The laser beam provides a light source for scattering and at the same time excites the fluorescent molecules used to label the cells.

After 5-MeV alpha-particle irradiation, adherent cells on the custom-made PADC cell dishes were trypsinized and these cells were collected from the cell dishes immediately. The collected cell suspensions were washed by phosphate buffered saline (PBS) and fixed. After permeabilisation, all the cells were washed with PBS. The cells were then resuspended in the TUNEL reaction mixture and incubated in dark for reaction to take place. Finally, the cells were analyzed by a flow cytometer to detect TUNEL signals that involve an excitation wavelength in the range of 450–500 nm (e.g., 488 nm) and detection in the range of 515–565 nm (green) Chan et al. (2007b, 2008). It was remarked that the TUNEL positive signals were determined relative to the negative signals measured by flow cytometer each time. Therefore,

all the steps for the TUNEL assay should be performed and all the reagents should be prepared on the same day. In this way, the number of samples used for determining TUNEL signals was inevitably restricted.

After the cells were trypsinized from the PADC film, the bottom side of the cell dish was etched by a 14 N KOH solution at 37 °C for 6 h to get sufficiently large tracks for identification of alpha-particle hit positions (Chan et al. 2007b, 2008). At this stage, there were no cells in the PADC cell dishes so a long etching time would not be a problem. After the second-time etching, two types of alpha-particle tracks appeared on the bottom side of a PADC film, namely, (1) 1 MeV alpha-particle tracks (markers) which had been etched for a cumulative period of 9 h 40 min (3 h 40 min + 6 h) and (2) 5 MeV alpha-particle tracks which had been etched for 6 h as shown here in Figure 4. Images of these tracks (hereafter referred to as the FT (final tracks) images) were captured. The FT images would be superimposed with the CM images previously captured through the alignment of the “base tracks” as markers.

An image of base tracks together with HeLa cells is shown in Figure 5(a). However, the cell nuclei cannot be seen clearly in this view as the focus is on the alpha-particle tracks developed on the bottom of the PADC film. Therefore, another image should be captured at the same position but with the focus on the cells, which is shown in Figure 5(b). By superimposing these two images using a photo editing software, both the cell nuclei and the tracks can be seen clearly.

The alpha-particle hit positions on the cells or otherwise can be determined from the superposition of CM images and FT images. An example is shown in Figure 6. Here, there are in fact three image layers, namely, (1) the layer with base tracks, (2) the layer with clear images of cell nuclei, and (3) the layer with enlarged base tracks and 5 MeV alpha-particle tracks. As demonstrated in Figure 6, the positions of alpha-particle hits by 5 MeV alpha particles on the cell nuclei could be determined by aligning the enlarged base tracks with the original base tracks. The number of alpha-particle hit cells can be obtained by counting the number of cells overlapping with the 5 MeV alpha-particle tracks. Moreover, the residual energies of the alpha particles that hit the cells would be dependent on the thickness of the pre-etched thin PADC film. For example, the original thickness of the thin PADC film corresponding to the residual energy of 0.39 MeV is  $29 \pm 1 \mu\text{m}$ . As a result, the final thickness of the thin PADC film is  $26.6 \mu\text{m}$  after 3 h 40 min etching. Finally, the residual energies were calculated using the SRIM program. The number of alpha particles hitting the cells and the energies of these alpha particles could be used as references to study the DNA strands broken by alpha-particle radiation.

Figure 7 gives a combined image of the area of cells hit by 5 MeV alpha particles with the enlarged base tracks. In this way, the number of alpha-particle hits on the cell nuclei can be counted. The preliminary results of Chan et al. (2007b) showed that more strand breaks occurred in cells hit by alpha particles with lower energies. Moreover, large TUNEL positive signals were obtained even with small percentages of cells irradiated, and TUNEL signals were also obtained from non-targeted cells. These provided evidence for the bystander effect.

### 3.2. PADC Cell Dishes for Alpha-Particle Irradiation of Zebrafish Embryos

It has been common to study DNA damage responses in vertebrates using *in vitro* cell cultures, such as those described in section 3.1 above. However, such experiments cannot be used to study dynamic *in vivo* processes such as temporally and spatially regulated patterns of gene expression (Geiger et al. 2006). In recent years, the zebrafish, *Danio rerio*, a small vertebrate from Southeast Asia, has become a preferred model for studying human disease, including carcinogenesis. The most important advantage is that the human and zebrafish genomes share considerable homology, including conservation of most DNA repair-related genes (Barbazuk et al. 2000). Rapid embryonic development is another advantage in that major organ systems become evident within 48 hours postfertilization (hpf).

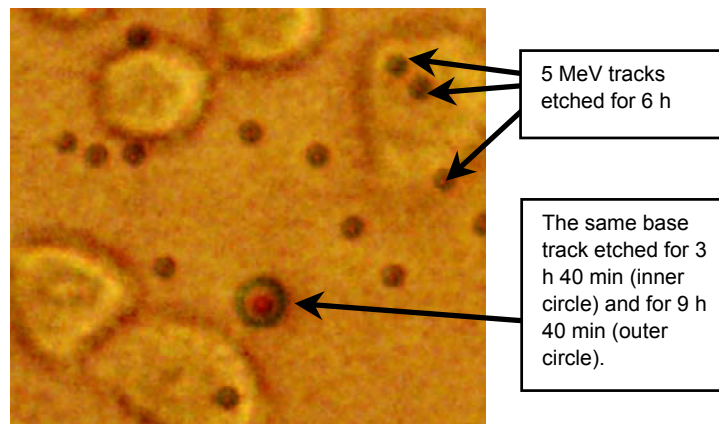


Figure 6. Superposition of the “cells and markers” image with the “final tracks” image through the alignment of the “base tracks” as markers. (Adopted from Chan et al. 2008.)

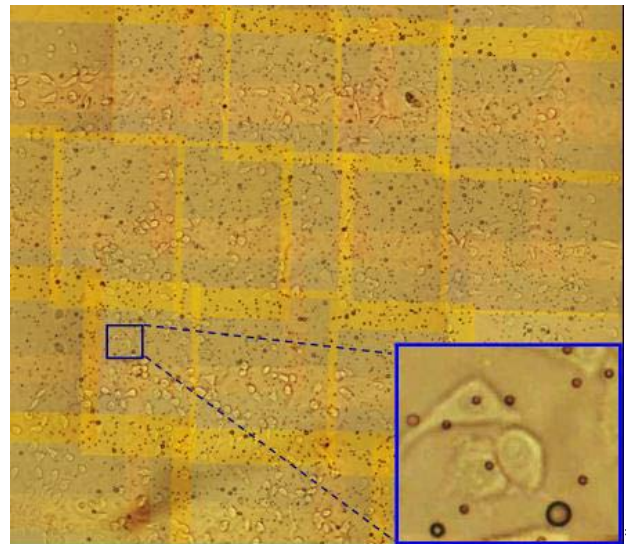


Figure 7. An overall image of the area of cells irradiated by 5 MeV alpha particles, together with base tracks from 1 MeV alpha particles. (Adopted from Chan et al. 2007b.)

Recently, a number of research works using the zebrafish embryo as an *in vivo* model to study the DNA damage response to ionizing radiation have emerged. For example, Bladen et al. (2005) studied the DNA damage response and Ku80 mRNA function in the zebrafish embryos irradiated with  $^{137}\text{Cs}$  gamma rays. McAleer et al. (2005) evaluated the effects of 250 kVp X-rays in combination with a known radioprotector (free radical scavenger Amifostine) or radiosensitizing agent (tyrosine kinase inhibitor AG1478) with a view to validate zebrafish embryos as a screen for radiation modifiers. McAleer et al. (2006) also used zebrafish embryos to study radiosensitizing effects of flavopiridol in normal tissues exposed to  $^{137}\text{Cs}$  gamma rays or 250 kVp X-rays. Daroczi et al. (2006) evaluated the radioprotective effect of the nanoparticle DF-1, which was a fullerene with antioxidant properties, in zebrafish embryos exposed to  $^{137}\text{Cs}$  gamma rays. Geiger et al. (2006) studied the effects of  $^{137}\text{Cs}$  gamma rays and concurrent treatment with Amifostine on the development of the zebrafish embryos. Despite the success of using the zebrafish embryos to study the DNA damage response to ionizing radiation in these studies, only energetic photons (X-rays and gamma rays) were used.

However, in order to study the DNA damage response to alpha particles using the zebrafish embryos, we have to solve two major problems. The first one concerns the absorption of alpha-particle energies in (a) the holder for the zebrafish embryos, (b) the fluid in which the zebrafish embryos are immersed, and (c) the chorions of the zebrafish embryos. By using the SRIM output results, it is noticed that significant portions of the alpha-particle energies can be absorbed in these three media. The second problem concerns the quantification of alpha-particle dose absorbed by the zebrafish embryo cells, which relies on the number of alpha particles actually incident on the embryo cells and the average energy of these alpha particles.

Yum et al. (2007) studied the feasibility of an experimental setup based on PADC films to tackle these two problems in order to study the effects of alpha particles on zebrafish embryos. To quantify the alpha-particle dose received by the zebrafish embryo cells, alpha-particle hit positions were needed. Yum et al. (2007) proposed to use PADC films as support substrates to record the positions where the alpha particles hit the embryos as shown in Figure 8.

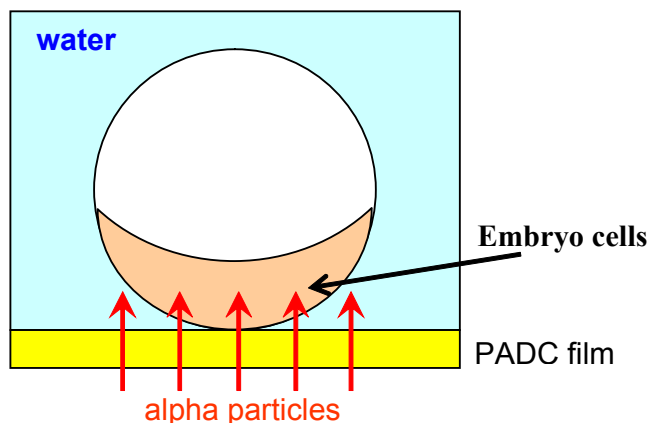


Figure 8. Schematic diagram showing alpha-particle irradiation of a zebrafish embryo, with the embryo cells resting on the bottom, and assuming that the alpha particles strike the PADC film vertically. (Adopted from Yum et al. 2007.)

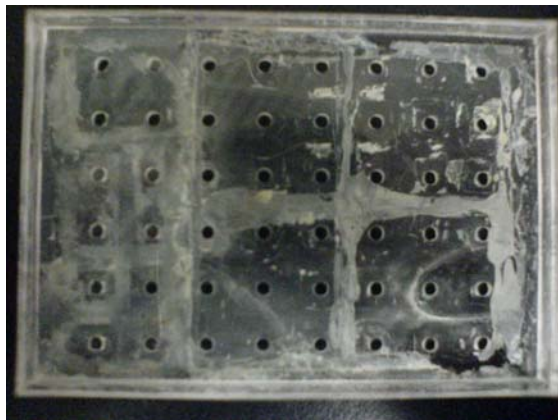


Figure 9. A custom-made PADC-film based holder for zebrafish embryos. (Adopted from Yum et al. 2007.)

For alpha-particle irradiation of zebrafish embryos, as is the case for alpha-particle irradiation of cells described in section 3.1 above, it is only feasible to quantify the alpha energies incident on the embryos if the alpha particles pass through the substrate to strike the embryo cells, because there is always a fluid layer with variable thickness above the embryos. The PADC substrate should then be thin enough to allow passage of alpha particles with nominal energies (e.g., those from  $^{241}\text{Am}$  source). Yum et al. (2007) prepared 16  $\mu\text{m}$  PADC films from commercially available CR-39 films following the procedures described in section 2. These thin PADC films were then glued by an epoxy to the bottom of a custom-made holder made of acrylic resin with  $8 \times 6$  holes drilled at the bottom. The holes had a diameter of 2 mm, and the holes were separated at 8 mm. A photo of the custom-made PADC-film based holder is shown in Figure 9.

The chorions of zebrafish embryos absorbed a significant fraction of the alpha-particle energies, so Yum et al. (2007) removed the chorions before alpha-particle irradiation. Dechorionated embryos were transferred to a petri-dish and were placed into the incubator and allowed to develop to 4 hours post fertilization (4 hpf). For alpha-particle irradiation, the dechorionated embryos were transferred into the custom-made PADC-film based holder shown in Figure 9, with 4 embryos in one hole. At 4 hpf, half of the embryos were irradiated for 4 min with alpha particles from a planar  $^{241}\text{Am}$  source from the side of the PADC film. The other half of the embryos without irradiation was taken as control samples. Images of the embryos were captured immediately after the alpha-particle irradiation, which would be employed to superimpose with the images of the alpha-particle tracks revealed after chemical etching to obtain the alpha-particle hit positions on the embryo cells (Yum et al. 2007).

After irradiating the embryos, all the embryos were labeled and separately transferred into individual containers and allowed to develop into 48 hpf. The PADC films were etched in 6.25 N NaOH at  $70^\circ\text{C}$  for 3 h. Images of the PADC films with visible alpha-particle tracks were captured with a digital camera attached to a microscope with a magnification of  $200\times$ . A total of 4 images covering different areas of a PADC film were taken and combined to reconstruct an overall image of the PADC film at the bottom of the hole as shown in Figure 10. The previous captured image of the embryos was then superimposed onto the current image (Yum et al. 2007). An example is shown in Figure 11.

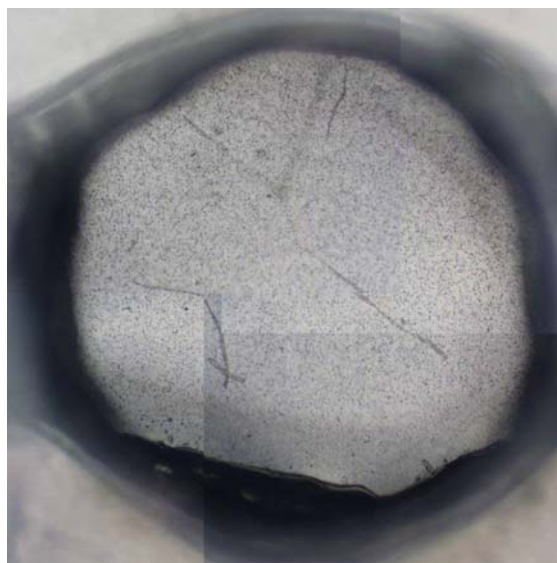


Figure 10. An overall image of a PADc film at the bottom of the hole with visible alpha-particle tracks, reconstructed from 4 images covering different areas. (Adopted from Yum et al. 2007.)



Figure 11. Superposition of (a) the image of the PADc film at the bottom of the hole with visible alpha-particle tracks shown in Figure 10 with (b) the image of embryos. (Adopted from Yum et al. 2007.)

However, not all the alpha particles traversing the PADc film could reach the embryo because some would lose all their energies while passing through the water column. By approximating an embryo as a sphere, Yum et al. (2007) determined the radius of the circular effective area containing alpha-particle tracks which corresponded to the alpha particles that could finally reach the embryos, and the number  $N_\alpha$  of these tracks was counted. The effective area was then plotted on the superimposed image of the embryo cells and the alpha particle tracks using the freely available image analyzing software called ImageJ (<http://rsb.info.nih.gov/ij/>).

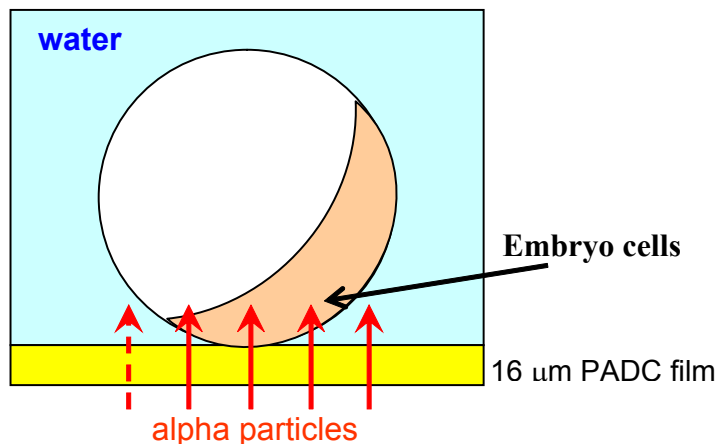


Figure 12. Schematic diagram showing alpha-particle irradiation of a tilted zebrafish embryo. The alpha particle represented by the dashed arrow does not hit embryo cells and should therefore be discarded when calculating the radiation dose. (Adopted from Yum et al. 2007.)

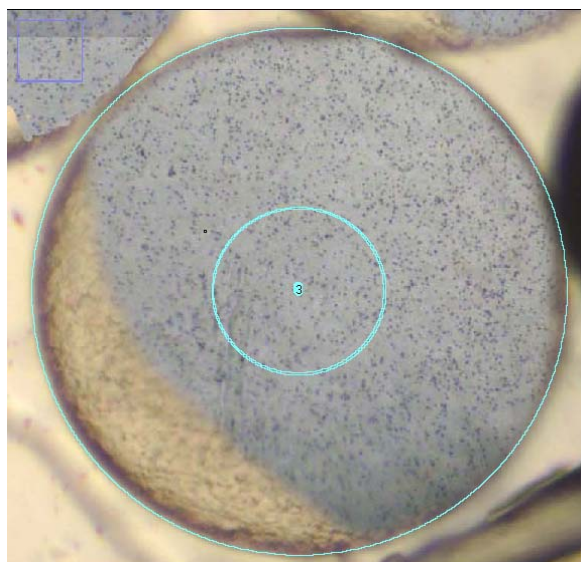


Figure 13. Outlines of the zebrafish embryo (outer circle) and the effective area (inner circle). The central dot represents the common center of the two circles. (Adopted from Yum et al. 2007.)

In general, however, it was difficult to rotate the embryos so that the embryo cells were exactly resting on the bottom. Instead, these embryos were more likely tilted as shown in Figure 12. In such cases, a part of the effective area may be void of embryo cells, and only the number of alpha-particle tracks ( $N_\alpha$ ) in the intersection between the effective area and the embryo cells should be counted. Figure 13 shows an example of the effective area drawn on a superimposed image of the embryo cells and the alpha particle tracks using ImageJ. Here, the effective area fell entirely in the area of the embryo cells, so all the tracks within the effective area should be counted to determine the radiation dose.

Images of the embryos at 48 hpf were captured for comparisons with the control samples and for identification of morphologic abnormalities. Three sets of experiments were carried

out on three separate days, with 20, 14 and 20 irradiated embryos and 17, 15 and 20 control embryos, respectively (Yum et al. 2007). Among the 54 irradiated embryos, 5 morphologic abnormalities were identified (2, 1 and 2 cases from the three sets), while no morphologic abnormalities were found in all the 52 control embryos. The rates of morphologic abnormalities were thus statistically significant ( $p = 0.011$ ) for irradiated and control embryos. Abnormal developments ranged from malformations in the tails to morphologic abnormalities in the whole body.

The number and energy of alpha particles incident on the embryo cells were required to compute the dose of alpha particles absorbed by the embryo cells. The energy of the alpha particles reaching the embryo cells varied according to the height of the water column they traveled. The counted track numbers corresponding to these 5 morphologically abnormal embryos were  $58 \pm 8$ ,  $64 \pm 8$ ,  $355 \pm 19$ ,  $155 \pm 13$ ,  $268 \pm 17$ , and the absorbed doses for 5 embryos were  $0.45 \pm 0.06$ ,  $0.41 \pm 0.05$ ,  $2.3 \pm 0.1$ ,  $0.58 \pm 0.05$  and  $1.1 \pm 0.1$  mGy (with the highest absorbed dose for all embryos as 2.3 mGy) (Yum et al. 2007).

Using the experimental setup for studying the effects of alpha particles on zebrafish embryos proposed by Yum et al. (2007) as described above, Yum et al. (2009) further studied the dose-risk relationship. As before, the embryos were dechorionated and transferred into a custom-made holder with a  $16 \mu\text{m}$  PADC film as the base. Alpha-particle irradiation was made with a planar  $^{241}\text{Am}$  source from the side of the PADC film at 1.25 hpf. The irradiation time was chosen as 30, 60 and 90s, and the average delivered doses to an embryo were calculated as 0.7, 1.4 and 2.1 mGy, respectively.

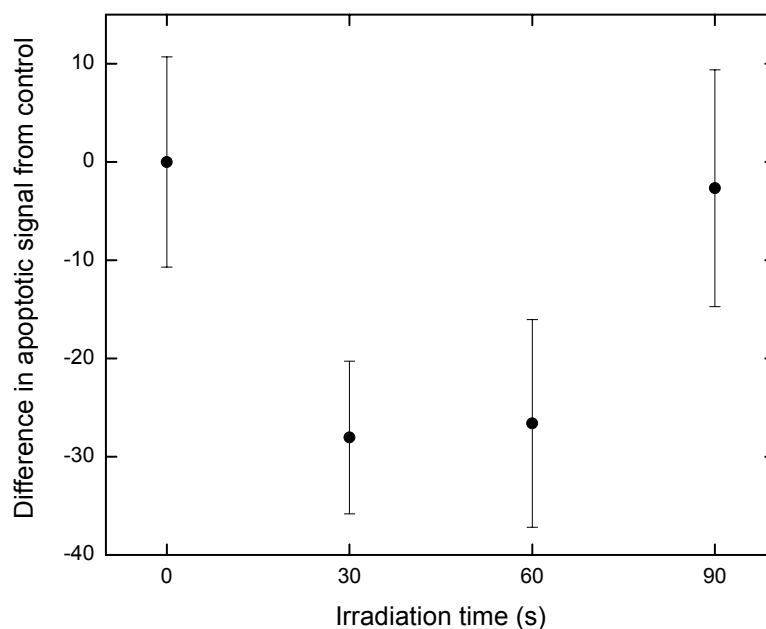


Figure 14. The mean difference ( $\pm$  SE) in the number of apoptotic cells obtained in embryos irradiated for different time and in the controls. (Adopted from Yum et al. 2009.)

After irradiation, the embryos were returned to the 37°C incubator until they developed into 24 hpf, which was their chosen endpoint for analyses of apoptosis, a highly regulated biological process during embryonic development. At 24 hpf, the embryos were collected and examined by vital dye staining using acridine orange (Chan and Cheng, 2003). Images of stained embryos were captured under a florescent microscope, and the number of apoptotic cells for each embryo was counted. The difference in the number of apoptotic cells obtained in embryos irradiated for different time and those in the corresponding controls were obtained and are reproduced here in Figure 14. The results showed a nonlinear dose-risk relationship and a reduction of risk at low doses, which did not support the “Linear No Threshold” hypothesis (Yum et al. 2007).

The above results demonstrate that zebrafish embryo is a feasible model for studying radiation response *in vivo*. Nevertheless, due to the random nature of alpha-particle emission, for the low doses used here, the numbers of alpha-particles traversing each cell and thus the resulting doses could vary to a large extent. This will be more serious if we explore the region for even smaller doses. Although it can be argued that bystander effects can distribute the effects so that all cells respond to the same extent, a microbeam facility will help avoid ambiguities caused by non-uniform doses, and help confirm such bystander effects *in vivo*.

## 4. BIOCOMPATIBILITY OF THE PADC FILM SUBSTRATE

### 4.1. Biocompatibility of Chemically Etched PADC Films

As described in section 1 above, the substrates for cell cultures should be biocompatible. Therefore, Li et al. (2006) studied the biocompatibility of raw PADC films and those etched using aqueous NaOH or NaOH/Ethanol through the abundance and morphology of HeLa cells cultured on them. PADC films with a thickness of 1000 µm were employed for their studies. The wetting properties of these PADC films were also studied through analyses of the contact angles, surface energies, and the polar and dispersive components.

To study the number of cells, to measure the contact angles and the surface energies, besides the raw SSNTDs, three sets of etched PADC films were prepared. These included (1) PADC films etched for 4 h in 6.25 N aqueous NaOH at 70°C, (2) PADC films etched for 1 h in 1 N NaOH/Ethanol at 40°C, and (3) PADC films first etched for 4 h in 6.25 N aqueous NaOH at 70°C and then for 1 h in NaOH/Ethanol at 40°C.

Li et al. (2006) found that the PADC film etched with NaOH/Ethanol had a similar biocompatibility (in terms of cell numbers) to the raw PADC film, while the PADC film etched with aqueous NaOH had a significant drop in the biocompatibility. Therefore, if thin PADC films are to be prepared from etching the commercially available thicker PADC films, NaOH/Ethanol is the preferred etchant. Interestingly, the PADC film first etched with aqueous NaOH and then with NaOH/Ethanol had a similar biocompatibility to the raw PADC film. It was apparent that the final step was more important in determining the biocompatibility of the etched PADC film. Therefore, if necessary, an alternative method to fabricate thin PADC films from etching PADC films is to first etch the films with aqueous NaOH and then with NaOH/Ethanol.

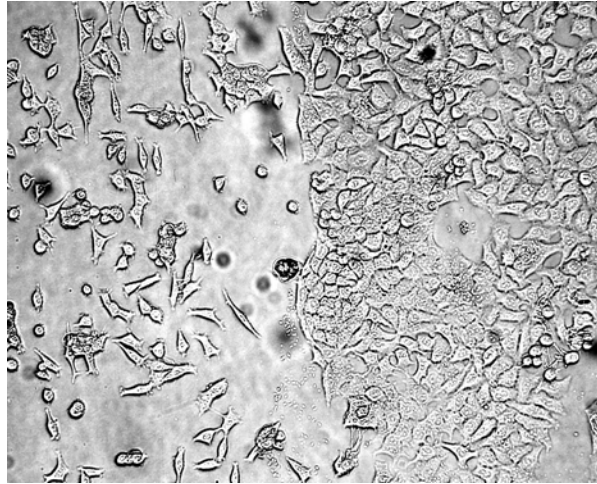


Figure 15. The image of HeLa cells cultured on a half etched PADc film captured under the optical microscope. The left side was etched for 4 h with 6.25N NaOH at 70°C while the right side was unetched. (Adopted from Li et al. 2006.)

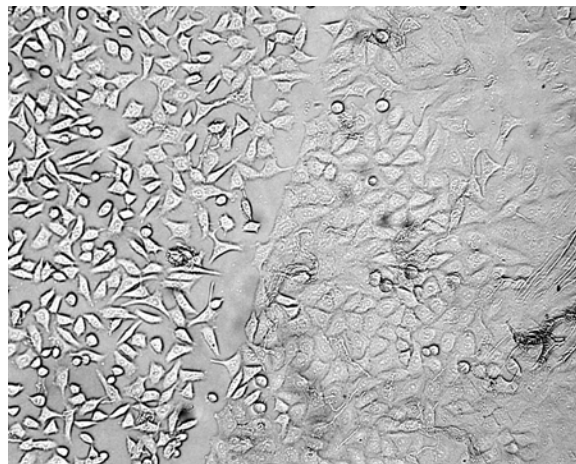


Figure 16. The image of HeLa cells cultured on a half etched PADc film captured under the optical microscope. The left side was etched for 1 h with 1N NaOH/Ethanol at 40°C while the right side was unetched. (Adopted from Li et al. 2006.)

To study the morphology of the cells, two types of specially etched PADc films were made (Li et al. 2006). For each of these films, one half was first masked by an epoxy adhesive and the whole film was then etched for 4 h in 6.25 N NaOH at 70 °C or etched for 1 h in 1 N NaOH/Ethanol at 40°C. The epoxy was then removed to expose the raw unetched surface. Effectively, PADc films half etched with aqueous NaOH or half etched with NaOH/Ethanol were obtained. The entire PADc films were then used for cell culture and the images of cells were captured under the optical microscope after 3 d of culture.

Figure 15 shows the image obtained by Li et al. (2006) of HeLa cells cultured on the PADc film half etched with aqueous NaOH and another half unetched. The first observation was the much smaller number of cells on the etched portion, which agreed with the above results on biocompatibility in terms of cell numbers. The second observation was that many

of the cells adhered on the etched portion were circular in shape while the cells cultured on the unetched portion had a high degree of spreading. The cells which did not spread did not strongly adhere to the film surface and were easily washed away by the PBS solution during cell counting. This also explained the small number of cells counted on the PADC film etched with aqueous NaOH.

Figure 16 shows the image obtained by Li et al. (2006) of cells cultured on the PADC film half etched with NaOH/Ethanol and another half unetched. The first observation was the similar number of cells on both the etched and unetched portions, which again agreed with the results on biocompatibility in terms of cell numbers. The second observation was that the cells cultured on the etched side had a high degree of spreading, although there seemed to be more cells circular in shape when compared to the unetched side. Li et al. (2006) then made a similar conclusion, i.e., NaOH/Ethanol was the preferred etchant to prepare thin PADC films from thicker PADC films.

Li et al. (2006) also investigated the wettability of raw and etched PADC films using the sessile drop technique using a contact angle goniometer. Measurements for contact angles and determination of the surface energy ( $\gamma_s$ ), polar component ( $\gamma_s^p$ ), dispersive component ( $\gamma_s^d$ ) and the ratio ( $\gamma_s^p/\gamma_s^d$ ) were performed for these PADC films in order to identify the relationships with the biocompatibility of the films. The results are shown in Table 2. PADC films etched in aqueous NaOH were hydrophilic (water contact angle of about  $39^\circ$ ), those etched in NaOH/Ethanol (water contact angle of about  $77^\circ$ ) or first etched in aqueous NaOH and then in NaOH/Ethanol (water contact angle of about  $75^\circ$ ) were hydrophobic, while the raw PADC films was in between (water contact angle of about  $60^\circ$ ). The surface energy  $\gamma_s$  was similar for raw and NaOH/Ethanol-etched PADC films (from 30 to  $40 \text{ mJ/m}^2$ ) but that for aqueous-NaOH-etched PADC films were distinctly higher ( $\sim 60 \text{ mJ/m}^2$ ). The polar component  $\gamma_s^p$  of the surface energy for aqueous-NaOH-etched PADC films ( $\sim 44 \text{ mJ/m}^2$ ) was also significantly higher. The moderately hydrophobic PADC films as well as the hydrophobic NaOH/ethanol-etched PADC films were more biocompatible than the hydrophilic aqueous-NaOH-etched PADC films. Too small water contact angles, too large surface energy ( $\gamma_s$ ) or the polar component ( $\gamma_s^p$ ) did not favor the cell culture. On the other hand, the dispersive component ( $\gamma_s^d$ ) of the surface energy and the ratio  $\gamma_s^p/\gamma_s^d$  did not seem to significantly affect the biocompatibility.

**Table 2. The contact angles measured for different PADC films using doubly distilled water (W), glycerol (G) and ethylene glycol (EG), and the determined surface energy ( $\gamma_s$ ), the polar ( $\gamma_s^p$ ) and dispersive ( $\gamma_s^d$ ) components, and the ratio ( $\gamma_s^p/\gamma_s^d$ ). (1) Raw PADC films; (2) PADC films etched for 4 h with 6.25N NaOH at  $70^\circ\text{C}$ ; (3) PADC films etched for 1 h with 1N NaOH/Ethanol at  $40^\circ\text{C}$ ; (4) PADC films etched for 4 h with 6.25N NaOH at  $70^\circ\text{C}$  and then for 1 h with NaOH/Ethanol at  $40^\circ\text{C}$ . (Adopted from Li et al. 2006)**

	W	G	EG	$\gamma_s$ ( $\text{mJ/m}^2$ )	$\gamma_s^p$ ( $\text{mJ/m}^2$ )	$\gamma_s^d$ ( $\text{mJ/m}^2$ )	$\gamma_s^p/\gamma_s^d$
1	59.9	58.3	40.1	40.9	28.8	12.1	2.38
2	39.2	35.1	10.1	57.7	44.3	13.4	3.30
3	76.5	67.9	46.0	32.7	10.0	22.7	0.44
4	75.0	68.7	52.7	30.4	14.4	16.0	0.90

## 4.2. Biocompatibility Enhancement of Chemically Etched PADC Films Through Superficial Pore Formation

In previous sections, thin PADC films with a thickness of 10 to 20  $\mu\text{m}$  have been proposed as cell-culture substrates for alpha-particle radiobiological experiments. Biocompatibility of the substrate is a key factor to the success of such radiobiological experiments. One of the main factors affecting the cell behavior is the surface topography (e.g., Baharloo et al. 2005). Ng et al. (2008a) explored biocompatibility enhancement of chemically etched PADC films through superficial pore formation by (pre-) alpha-particle irradiation.

PADC films treated differently were employed for culturing HeLa cells, including raw PADC films which were not etched, and both unirradiated and irradiated PADC films which were subsequently chemically etched. The irradiated PADC films were prepared by irradiation with 3 MeV alpha particles from an  $^{241}\text{Am}$  alpha-particle source for 3 h (giving an average track density of  $415000 \text{ tracks cm}^{-2}$ ). Both unirradiated and irradiated PADC films were etched for 15, 29 and 60 min in 6.25 N aqueous NaOH at 70  $^{\circ}\text{C}$ , and then for 5 min in 1 N NaOH/ethanol at 40  $^{\circ}\text{C}$ . The etching conditions produced superficial pores with sizes which were small compared with the cell dimensions. The films were etched in NaOH/ethanol in the end because Li et al. (2006) found that the NaOH/ethanol-etched PADC films were more biocompatible than the NaOH/H<sub>2</sub>O-etched PADC films (see also section 3.1 above).

To characterize the surface topography of the irradiated and etched PADC films, the size of the superficial pores were determined using AFM. The numbers of cells cultured on these detectors, the average cell area, as well as the cell morphology were then determined, which were used as indicators for the biocompatibility (Li et al. 2006).

For short etching time (15 min) in NaOH/H<sub>2</sub>O (with subsequent etching in NaOH/ethanol), the biocompatibility of the PADC film was enhanced through superficial pore formation by alpha-particle irradiation. In contrast, for long etching time (60 min) in NaOH/H<sub>2</sub>O (with subsequent etching in NaOH/ethanol), the biocompatibility of the PADC film deteriorated through superficial pore formation.

In a related follow-up study, Ng et al. (2008b) further examined the topographical effects on cell behavior using micrometer-size pits on the surface of a PADC substrate created by alpha-particle irradiation and subsequent chemical etching. Vinculin, the cell adhesion and membrane protrusion protein, was used as an indicator of cytoskeletal reorganization on the substrate and localization of vinculin was used to demonstrate the presence of focal adhesions. Ng et al. (2008b) found that vinculin expressed in the HeLa cells cultured on PADC films with track-etch pits, but not in cells cultured on the raw or chemically etched blank films. In other words, vinculin expression was induced by the topography of track-etch pits, while etching of the substrate alone (without alpha-particle irradiation) did not cause up-regulation of vinculin protein expression.

Figure 17A shows the expression of vinculin on HeLa cells cultured on the PADC films subjected to different treatments. In Figure 17A, the images from confocal microscope, the transmission mode optical images as well as their superpositions are shown. From Figure 17A, we observe overall increases in vinculin expression for HeLa cells cultured on PADC films with track-etch pits. On the contrary, vinculin-rich regions were not revealed in cells cultured on the raw (unetched) as well as the blank (etched) PADC films. Figure 17B

illustrates the expression of vinculin. Here, representative images from western blotting are shown, where the size of vinculin protein is about 117 kDa. The respective bands which represent the expression of vinculin from proteins sampled from HeLa cells cultured on PADC films with track-etch pits were stronger than those for cells cultured on the raw (unetched) as well as on the blank (etched) PADC films. The results for cells cultured on track-etch pits and those cultured on the raw detectors were found to be statistically significant ( $p < 0.05$ ).

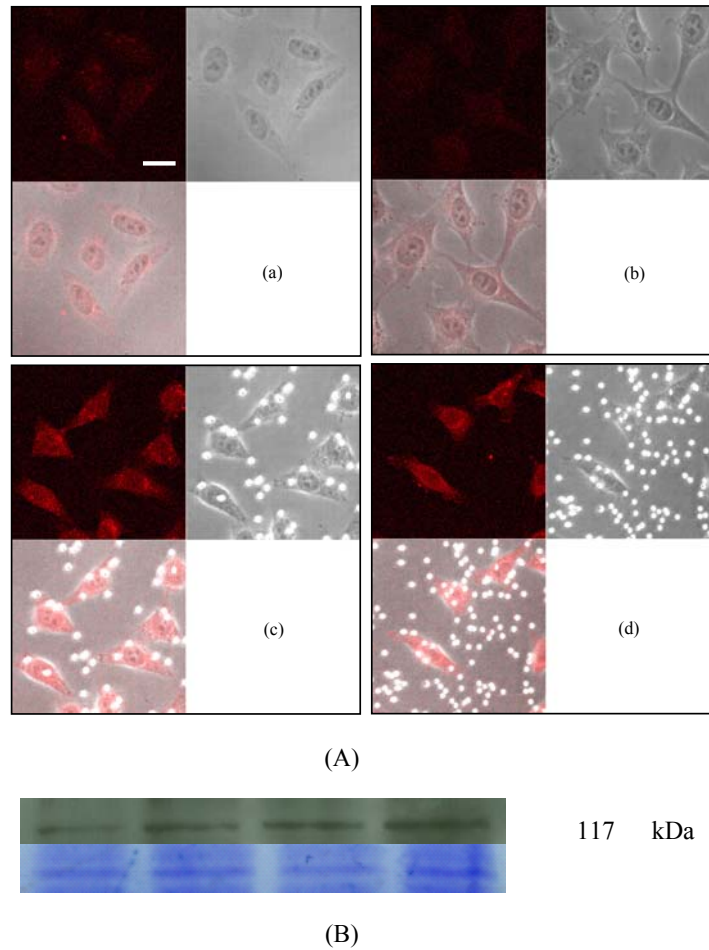


Figure 17. (A) Representative images showing the spatial expression of vinculin on HeLa cells on (a) raw and unetched PADC film; (b) etched blank PADC film; (c) PADC film irradiated by 3 MeV alpha particles for 3 h and etched; (d) PADC film irradiated by 3 MeV alpha particles for 6 h and etched. For (b), (c) and (d), etching was performed for 3 h in 6.25 N aqueous NaOH at 70 °C and then for 5 min in 1 N NaOH/ethanol at 40 °C. Bar = 20  $\mu$ m; n = 3; (a) to (d) are at identical magnification. For (a) to (d), upper left: images from confocal microscope; upper right: transmission mode optical images; lower left: superposition of the upper left and upper right images. (B) Vinculin detected by immunoblot presented as fold changes. Upper image lanes: 1, blank and unetched film; 2, 3h etched blank film; 3, etched film with 3 h irradiation; 4, etched film with 6 h irradiation. Right margin arrow, molecular weight standard. Below, identically loaded Coomassie-stained gel (loading controls). Lanes 3 and 4 showed statistically significant increases compared with raw (\*  $p < 0.05$ , mean+SD, n=3). (Adopted from Ng et al. 2008b)

HeLa cells cultured on PADC films with track-etch pits also showed changes in cell proliferation, cell area and cell circularity, and were largely contained by the pits (Ng et al. 2008b). In other words, the cell membrane edges tended to be in contact with the pits. By comparing the correlation between the positions of HeLa cells and the pits, and that between the positions of cells and computer-simulated pits, the tendency for membrane edges of HeLa cells to be in contact with the pits was recognized. This could be explained by inhibition of membrane protrusion at the pits (Ng et al. 2008b). In conclusion, substrate track-etch pits were an important determinant of epithelial cell behaviors.

## REFERENCES

- Baharloo, B; Textor, M; Brunette, DM. *J. Biomed Mater Res.*, 2005, 74A, 12-22.
- Barbazuk, WB; Korf, I; Kadavi, C; Heyen, J; Tate, S; Wun, E; Bedell, JA; McPherson, JD; Johnson, SL. *Genome Res.*, 2000, 10, 1351-1358.
- Bladen, CL; Lam, WK; Dynan, WS; Kozlowski, DJ. *Nucleic Acids Res.*, 2005, 33, 3002-3010.
- Chan, KF; Tse, AKW; Fong, WF; Yu, KN. *Nucl Instrum Meth B*, 2006, 247, 307-312.
- Chan, KF; Lau, BMF; Nikezic, D; Tse, AKW; Fong, WF; Yu, KN. *Nucl Instrum Meth B*, 2007a, 263, 290-293.
- Chan, KF; Yum, EHW; Wan, CK; Fong, WF; Yu, KN. *Nucl Instrum Meth B*, 2007b, 262, 128-134.
- Chan, KF; Yum, EHW; Wan, CK; Fong, WF; Yu, KN. *Radiat Measur.* 2008, 43 (Suppl. 1), S541-S545.
- Chan PK; Cheng, SH. *Arch. Toxicol.*, 2003, 77, 69-79.
- Daroczi, B; Kari, G; McAleer, MF; Wolf, JC; Rodeck, U; Dicker, AP. *Clin Cancer Res.*, 2006, 12, 7086-7091.
- Durante, M; Grossi, GF; Pugliese, M; Manti, L; Nappo, M; Gialanella, G. *Nucl Instr Meth B.*, 1994, 94, 251-258.
- Dorschel, B; Hermsdorf, D; Pieck, S; Starke, S; Thiele, H; Weickert, F. *Nucl Instr Meth B.*, 2003, 207, 154-164.
- Gaillard, S; Ross, CJ; Armbruster, V; Hill, MA; Stevens, DL; Gharbi, T; Fromm, M. *Radiat Measur.*, 2005, 40, 279-282.
- Gaillard, S; Pusset, D; de Toledo, SM; Azzam, EI; Fromm, M. *Radiat Measur.*, 2008, 43, S34-S40.
- Geiger, GA; Parker, SE; Beothy, AP; Tucker, JA; Mullins, MC; Kao, GD. *Cancer Res.*, 2006, 66, 8172-8181.
- Li, WY; Chan, KF; Tse, AKW; Fong, WF; Yu, KN. *Nucl Instr Meth B.*, 2006, 248, 319-323.
- McAleer, MF; Davidson, C; Davidson, WR; Yentzer, B; Farber, SA; Rodeck, U; Dicker, AP. *Int J Radiat Oncol Biol Phys.*, 2005, 61, 10-13.
- McAleer, MF; Duffy, KT; Davidson, WR; Kari, G; Dicker, AP; Rodeck, U; Wickstrom, E. *Int J Radiat Oncol Biol Phys.*, 2006, 66, 546-551.
- Ng, CKM; Chan, KF; Li, WY; Tse, AKW; Fong, WF; Cheung, T; Yu, KN. *Radiat Measur.*, 2008a, 43 (Suppl. 1), S537-S540.

Ng, CKM; Poon, WL; Li, WY; Cheung, T; Cheng, SH; Yu, KN. *Nucl Instr Meth B*, 2008b, 266, 3247-3256.

Nikezic, D; Yu, KN. *Mat Sci Eng R*, 2004, 46, 51-123.

Tse, KCC; Nikezic, D; Yu, KN. *Nucl Instr Meth B*, 2007, 263, 300-305.

Yum, EHW; Ng, CKM; Lin, ACC; Cheng, SH; Yu, KN. *Nucl Instr Meth B*, 2007, 264, 171-176.

Yum, EHW; Cheng, SH; Yu, PKN. *J Radiat Res.*, 2009, 50 Suppl. A, A93.